Journal of Electronic Materials
https://doi.org/10.1007/s11664-024-11584-x

TOPICAL COLLECTION: ELECTRONIC PACKAGING AND INTERCONNECTION MATERIALS 2024

The Effect of Gallium Addition on the Microstructure and Superconducting Properties of In-Bi-Sn Solder Alloys

Jiye Zhou[1] · Mahboobeh Shahbazi[2] · Jordan T. Poitras[3] · Xin Fu Tan[1] · Stuart D. McDonald[1] · Kazuhiro Nogita[1]

Received: 9 July 2024 / Accepted: 29 October 2024

Abstract
Ternary In-Sn-Bi alloys exhibit potentially superior superconducting properties compared to other lead-free solders, making them promising candidates for replacing lead-based solders in superconducting joints. In this work, the microstructure and superconducting properties of In-15wt.%Bi-35wt.%Sn and In-23wt.%Bi-27wt.%Sn were studied and compared with samples containing 0.5 wt.% and 1 wt.% Ga addition. The study reveals significant modifications in the microstructure with the addition of Ga, resulting in a slight decay in superconducting properties when higher levels of liquid Ga are present in the microstructure. Moreover, the difference in superconducting properties between the two In-Bi-Sn compositions is negligible, despite different microstructures. The highest critical temperature of 6.76 K was achieved in In-23wt.%Bi-27wt.%Sn. The tested superconducting properties including critical temperature (T_c), critical current density (J_c) and critical magnetic field strength (H_c) are discussed with respect to pinning mechanisms and microstructures based on electron backscatter diffraction (EBSD) and x-ray diffraction (XRD) results.

Keywords Superconducting joints · low-temperature solder · In-Sn-Bi alloys · electronics packaging

Introduction

The quest for developing lead-free superconducting solders for nuclear fusion reactors and particle accelerators has intensified recently, driven by environmental concerns and regulatory restrictions on lead usage.[1–3] Traditional lead-based solders are effective but pose significant health and environmental risks due to the toxicity of lead. Typically, lead-based alloys are widely used as superconducting solders; for example, the Pb-45Sn alloy (compositions are in wt.% unless specified otherwise) has a critical temperature $T_c = 7.2$ K,[4] while a $T_c = 8.4$ K and critical magnetic field strength H_{c2} (4.2 K) = 1.77 T was reported in the Pb-40Bi alloy.[5,6] As the superconducting properties of lead-based solder alloys are better than those of lead-free solder alloys, it is necessary to develop a new green alloy that satisfies stringent requirements including low melting point, good wettability and excellent superconducting properties under operational conditions, usually at cryogenic temperatures.

Recent studies have turned their focus towards indium-based solder alloy systems, which show promising superconducting properties, potentially outperforming other lead-free candidates. The eutectic In-48Sn alloy has a relatively high $T_c = 5.4$ K, and with Bi addition in the alloy, a $T_c = 6.9$ K was reported in In15Bi35Sn.[7] It has been revealed that the In-25Sn alloy, consisting of a 100% β phase in the microstructure, has a maximum T_c of 6.3 K after quenching,[8] compared to a T_c of 4.3 K detected in In-75Sn, which has a 100% γ phase.[8] Therefore, the β phase plays an important role in improving the superconducting properties in the In-Sn binary system or In-Sn-Bi ternary system. The β phase is stable over a wide composition range of Sn and In, while the addition of Bi solute atoms adds to the variations in composition and therefore modifies the superconducting properties.[9] Furthermore, it has been reported that with

✉ Xin Fu Tan
xin.tan@uq.edu.au

1 School of Mechanical and Mining Engineering, The University of Queensland, St. Lucia, QLD 4072, Australia

2 School of Chemistry and Physics and Centre for Materials Science, Queensland University of Technology, Brisbane, QLD 4000, Australia

3 Centre for Microscopy and Microanalysis, The University of Queensland, St. Lucia, QLD 4072, Australia

the increase of Sn solute atoms in β solid solution through quenching the sample, the superconducting properties were further improved,[7,9] where a maximum $T_c = 7.3$ K was detected in an In-30wt.% Sn alloy.[10]

Trace element additions can change the microstructure significantly and further influence the solders' superconducting properties. For instance, the addition of 5 wt.% Sb to In-35wt.%Sn and In-65wt.%Sn alloys can improve the overall superconducting properties as Sb acts as a solute atom that dissolves into the crystalline lattice of β and γ phases.[9] Furthermore, with the addition of Nb, Pb, AgCu intermetallic and graphene in In-35wt.%Sn solder alloys, the critical temperature increased slightly.[11] It has been reported that Ga-In-Sn liquid alloys have a superconducting critical temperature (T_c) of 6.28 K,[12] while the effect of small Ga additions on the superconducting properties of In-Sn-Bi solder alloys remains unknown. As the microstructure, volume fraction and composition of each phase can be manipulated to achieve better superconducting properties such as higher T_c, critical field (B_{c2}) and critical current density (J_c), it is worth investigating the effect of gallium additions on superconducting properties and microstructural changes.

In this work, the microstructure and superconducting properties of In-15wt.%Bi-35wt.%Sn and In-23wt.%Bi-27wt.%Sn alloys, which have a different volume fraction of β phase, were investigated. The effect of Ga addition and how it influences the superconducting properties are discussed in relation to the variations in the microstructure.

Experimental Procedure

Superconducting Properties

For superconducting properties, all the tested samples including In-15wt.%Bi-35wt.%Sn, In-23wt.%Bi-27wt.%Sn and those with 0.5 wt.% and 1 wt.% Ga addition were alloyed at 300°C using pure indium (99.995%) ingots (supplied by Nihon Superior Co., Ltd., Japan), tin (99.99%) ingots, bismuth (99.99%) ingots (supplied by Northern Smelters, Woodridge, QLD, Australia) and pure gallium in a clay-graphite crucible. Melted samples were solidified between two glass plates and then cut into pieces of approximately 0.2×0.3×0.05 cm.

Zero-field-cooled (ZFC) and field-cooled (FC) magnetisation (M) curves as a function of temperature were measured at 100 Oe using a Cryogenic Ltd Mini Cryogen Free System (Cryogenic Ltd, London, UK) with a 5T magnet. T_c (critical temperature) was determined as the intersection of linearly extrapolated $M(T)$ with the $M =$ constant line. Magnetic hysteresis loops were measured at 3 K for all samples. The temperature dependence of resistance was carried out using a four-point contact configuration from room temperature down to 4 K at a rate of 0.4 K/min. Subsequently, the sample was heated from 4 K to room temperature at a rate of 5 K/min.

Microstructural Analysis

Microstructural characterisation was carried out using analytical scanning electron microscopy (SEM) (Hitachi SU3500-A) for In-23wt.%Bi-27wt.%Sn, In-15wt.%Bi-35wt.%Sn and those with 1 wt.% Ga for each composition. Small pieces of cast samples were prepared using an ion milling machine (Hitachi IM4000Plus Ion Milling System) to obtain a clean surface finish. Each sample underwent ion milling for a total of 6 min, with a 1-min interval off after 3 min. The ion milling machine was set to 3 kV accelerating voltage and 3.5 mm eccentricity with a 50° ion beam irradiation angle. Samples were further cleaned by a plasma cleaner (Evactron 25 De-Contaminator RF Plasma Cleaning System) before SEM analysis. The microstructure images of the prepared samples were captured under backscatter electron (BSE) mode at a 20 kV accelerating voltage.

In-23wt.%Bi-27wt.%Sn was selected as a representative sample for electron backscatter diffraction (EBSD) analysis to further understand the relationship between microstructure and superconducting properties. An ion beam cross-section polisher (JEOL IB-19530CP) was used for preparing the In-23wt.%Bi-27wt.%Sn EBSD sample, the machine was set to 8 s of beam on and 30 s beam off using a 2 kV accelerating voltage to polish a cross-section surface for a total of 6 h. The EBSD analysis was performed at a voltage of 20 kV on a JEOL JSM-7800F SEM equipped with an Oxford Instruments HKL EBSD system.

Solidification and Phase Characterisation

The thermal properties of the In-15wt.%Bi-35wt.%Sn, In-23wt.%Bi-27wt.%Sn and those with 0.5 wt.% and 1 wt.% Ga additions were tested using a differential scanning calorimetry (DSC) machine (TA Discovery DSC 2500). Approximately 10 ± 1 mg samples were sealed into Tzero aluminium pans and lids (Waters Australia Pty Ltd) for measurement. These samples were heated from 20°C to 120°C, then cooled to −90°C using a cryo cooling unit under a ramp rate of 10°C/min.

For x-ray diffraction (XRD) analysis, bulk samples were analysed on a Bruker D8 Advance x-ray diffractometer equipped with a Cu anode, operated at 40 kV and 40 mA. A Lynxeye XE energy discriminating 2D array detector was used to minimise fluorescent backgrounds and an automated knife edge was used to allow measurements at low and high angles. Diffraction patterns were recorded by continuous scans from 10° to 80° 2Θ. Results were imported into DIFFRAC.EVA version 5.1 and Rietveld refinement

was performed by TOPAS V6 software (Bruker AXS, Germany) using lattice parameters from the PDF-5 2024 ICDD database (In_3Sn-04-002-9972; $InSn_4$-00-048-1547; $BiIn_2$-00-011-0566).

Results and Discussion

Solidification and Phase Characterisation

Figure 1 shows the DSC heating (from room temperature to above the liquidus temperature of the sample) and cooling (down to 0°C) curves of the In-15wt.%Bi-35wt.%Sn and In-23wt.%Bi-27wt.%Sn samples, with and without Ga additions. As shown in the In-Sn-Bi phase diagram (see Fig. 2), the ternary alloys (Ga-free) have microstructures that contain three phases including β (In_3Sn), γ ($InSn_4$) and $BiIn_2$. Three endothermic peaks were detected for In-15wt.%Bi-35wt.%Sn and In-23wt.%Bi-27wt.%Sn (as shown in Fig. 1a and c), where the two peaks at higher temperatures are associated with the melting of primary γ and $\beta+\gamma$, respectively, and the peak at the lowest temperature is associated with the melting of eutectic phases. As shown in Fig. 1, the Ga addition in both In-15wt.%Bi-35wt.%Sn and In-23wt.%Bi-27wt.%Sn samples reduce the liquidus temperatures during solidification and melting. For the In-15wt.%Bi-35wt.%Sn, with 1 wt.% Ga addition, the liquidus temperature decreased from around 102°C to 96°C. We suspect that the addition of Ga acts as a nucleation inhibitor, altering the crystallisation kinetics by changing the solubility of Sn or Bi in the liquid phase during solidification, thereby shifting the formation of the γ phase to lower temperatures. With increasing Ga addition, the exothermic peaks related to the formation of the primary γ phase and the $\gamma+\beta$ phases become narrower for both compositions. The onset temperatures of these exothermic peaks shift to lower temperatures to varying degrees as

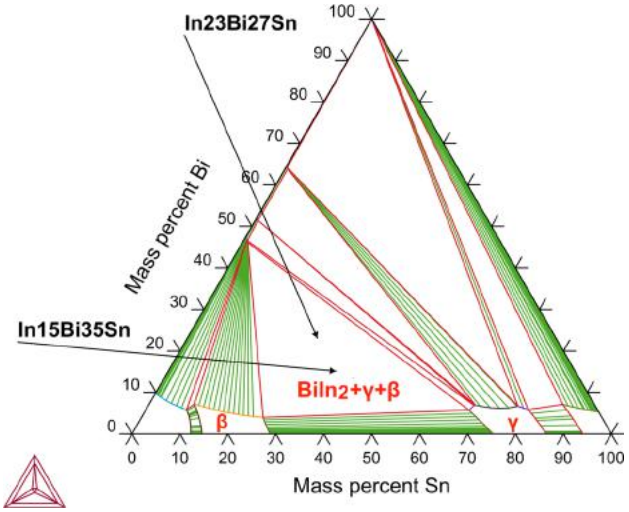

Fig. 2 In-Bi-Sn ternary phase diagram at 20°C calculated based on the Thermo-Calc 2024a[15] database (TCSLD4: Solder Alloy v4.1) with alloy compositions studied in this work.

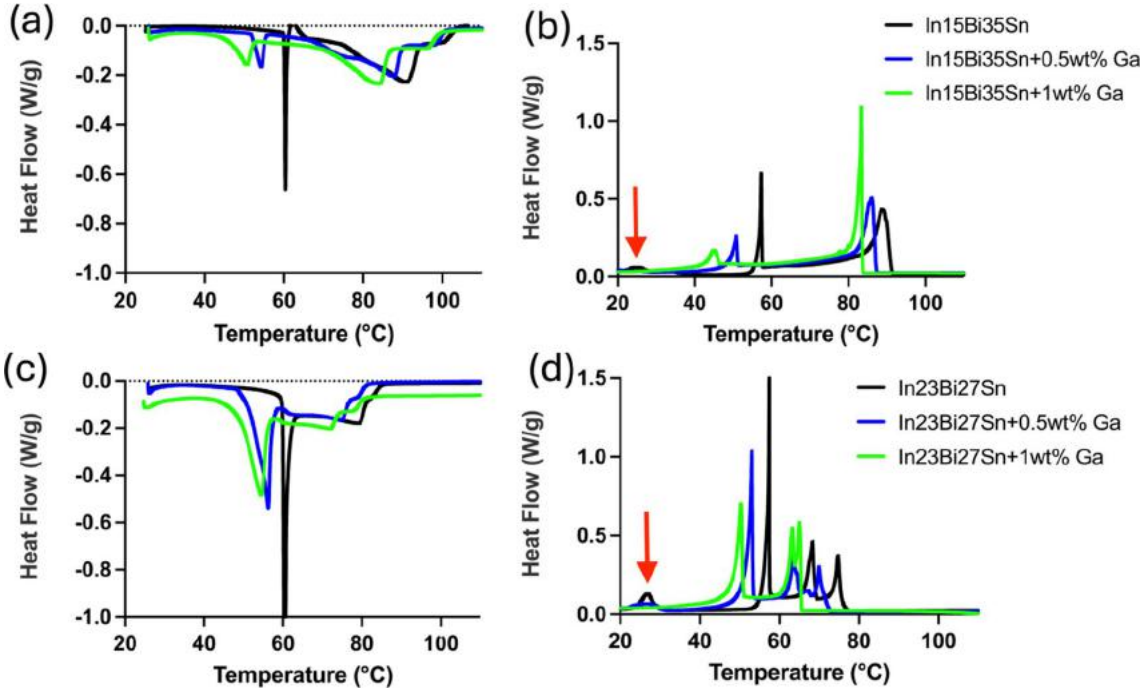

Fig. 1 DSC curves of tested samples. (a) and (b) Endothermic peaks and exothermic peaks of In-15wt.%Bi-35wt.%Sn samples; (c) and (d) endothermic peaks and exothermic peaks of In-23wt.%Bi-27wt.%Sn samples (Color figure online).

summarised in Table I, indicating that undercooling occurs during these reactions in these solder alloys. Several pieces of evidence suggest that Ga influences the undercooling of the solders during solidification.

From Table I and by comparing Fig. 1c and d, it is observed that the temperature difference between the first and second exothermic peaks, associated with the formation of primary γ and $(\beta+\gamma)$, decreases, and the solidification temperature is significantly reduced. This undercooling associated with the formation of the primary γ phase and $(\beta+\gamma)$ is more pronounced in the In-23wt.%Bi-27wt.%Sn series than the In-15wt.%Bi-35wt.%Sn series. In contrast, undercooling of the eutectic reaction in both series is minimal.

In comparison, as shown in Fig. 1a and b, for the In-15wt.%Bi-35wt.%Sn series, two endothermic peaks were detected at approximately 100°C and 90°C, which are related to the melting of primary γ and $\beta+\gamma$ during heating. However, the exothermic peak associated with the formation of the γ phase is absent during cooling.

Furthermore, a peak associated with phase transformation between $BiIn_2$ and β or γ, as well as solute redistribution can be detected at around 25°C for both samples without Ga addition during cooling. However, with Ga addition, the phase transformation at lower temperatures is suppressed, and solute redistribution becomes more difficult. This can be attributed either to a modified reaction associated with the formation of $BiIn_2$ occurring around 45°C, or to the presence of Ga at the grain boundaries, which hinders diffusion. Further research is required to understand the impact of Ga on the solute atom distribution in these three phases, as well as the relationship between undercooling and grain refinement with the addition of Ga, which is crucial for the development of advanced solder alloys.

The XRD patterns of the tested samples are displayed in Fig. 3. For all tested samples, three phases β(In-rich phase), γ(Sn-rich phase) and $BiIn_2$(Bi-rich phase) were identified by XRD. Notably, there is no peak associated with Ga, indicating either Ga exists in the liquid phase within the microstructure at room temperature or the small amount of Ga addition is difficult to detect by the XRD. Depending on the composition, the peaks of the γ and β phase in the In-23wt.%Bi-27wt.%Sn and the In-15wt.%Bi-35wt.%Sn samples shift from the positions of stoichiometric β-In_3Sn and γ-$InSn_4$ simulated from the PDF files, indicating lattice shrinkage or expansion along different axes, which is consistent with our previous study.[13] The Sn, In and Bi atoms have an atomic radius of 0.145 nm, 0.155 nm and 0.160 nm,[14] respectively. Due to the differences in radii, atomic interactions can cause changes in lattice parameters at off-stoichiometric compositions. With the addition of Ga, the β and γ peaks in both samples shift slightly to the higher 2Θ relative to those in the Ga-free samples (Fig. 3a and b). Therefore, the addition of Ga may alter the composition of each phase, likely by reducing the proportion of the larger Bi and/or In solute atoms dissolved in the γ and β phases. This can be verified by the Rietveld refinement results shown in Table II. For both samples, the lattice parameters of the γ phase along both the *a*-axis and *c*-axis show a notable decrease with the addition of 1 wt.% Ga. Specifically, the *a*-axis and *c*-axis of the γ phase in In-23wt.%Bi-27wt.%Sn-1wt.%Ga decreased by 0.16% and 0.21%, respectively, while in In-15wt.%Bi-35wt.%Sn-1wt.%Ga, the lattice parameters decreased by 0.09% and 0.14%. Additionally, with 1 wt.% Ga, there is a significant reduction in the lattice parameter of the β phase along the *c*-axis, while the *a*-axis shows negligible change. In contrast, the lattice parameters of the $BiIn_2$ (Sn) phase show a slight increase for both samples. Overall, these variations in lattice parameters can be attributed to the different distribution behaviours of solute atoms, such as Bi in the β/γ phases or Sn in the $BiIn_2$(Sn) phase, with or without Ga addition. Comparing the samples with Ga addition (Fig. 3c and d) to those without Ga addition (Fig. 3a and b), there is an increase in relative peak intensity of the γ and/or $BiIn_2$ phases with a decrease in the β phase at the same time. This indicates a reduction in the volume fraction of the β phase, which is considered a good superconducting phase, and suggests the β phase transforms into the γ phase and $BiIn_2$ in the microstructure of the samples with Ga addition. As the γ phase has the worst superconducting properties among all three phases,[7,8] with a volume fraction change between each phase as well as a lower number of solute

Table I Undercooling of phases

	Eutectic undercooling (°C)	$\beta+\gamma$ undercooling (°C)	Primary γ undercooling (°C)
In-15wt.%Bi-35wt.%Sn	3.1	1.6	Not observed
In-15wt.%Bi-35wt.%Sn + 0.5wt.%Ga	3.4	1.5	Not observed
In-15wt.%Bi-35wt.%Sn + 1wt.%Ga	5.4	0.6	Not observed
In-23wt.%Bi-27wt.%Sn	3.0	13.5	19.1
In-23wt.%Bi-27wt.%Sn + 0.5wt.%Ga	3.2	18.3	23.9
In-23wt.%Bi-27wt.%Sn + 1wt.%Ga	4.0	15.6	18.0

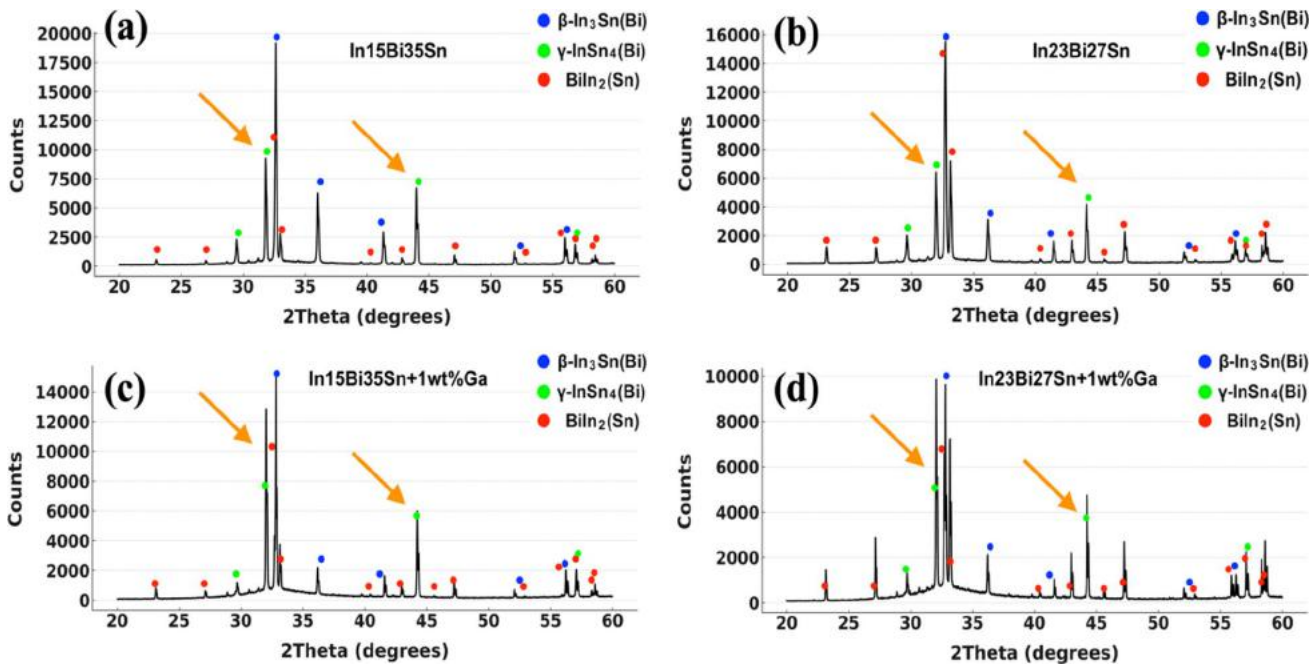

Fig. 3 XRD patterns of tested samples from 20° to 60°. (a) In-15wt.%Bi-35wt.%Sn; (b) In-23wt.%Bi-27wt.%Sn; (c) In-15wt.%Bi-35wt.%Sn with 1wt.%Ga addition; (d) In-23wt.%Bi-27wt.%Sn with 1wt.%Ga addition (Color figure online).

Table II Lattice parameters of each phase in tested samples

	a-axis (Å)	Change in *a*-axis (%)	*c*-axis (Å)	Change in *c*-axis (%)	Phase
In-23wt.%Bi-27wt.%Sn	3.5178		4.3585		*β*
	3.2361		3.0202		*γ*
	5.4821		6.5866		$BiIn_2(Sn)$
In-23wt.%Bi-27wt.%Sn + 1wt.%Ga	3.5169	−0.03	4.3498	−0.20	*β*
	3.2309	−0.16	3.0138	−0.21	*γ*
	5.4862	+0.07	6.5881	+0.02	$BiIn_2(Sn)$
In-15wt.%Bi-35wt.%Sn	3.5147		4.3565		*β*
	3.2338		3.0183		*γ*
	5.4817		6.5783		$BiIn_2(Sn)$
In-15wt.%Bi-35wt.%Sn + 1wt.%Ga	3.5163	+0.04	4.3490	−0.17	β
	3.2309	−0.09	3.0141	−0.14	γ
	5.4862	+0.08	6.5853	+0.11	$BiIn_2(Sn)$

atoms in the lattice, a decay of superconducting properties is observed in samples with Ga addition (see Figs. 4 and 6).

Critical Temperature and Microstructural Analysis

The tested critical temperature T_c of each sample is labelled on the corresponding microstructure in Fig. 4. The microstructure of the samples reveals distinct differences in phase distribution and significant morphology changes that occur due to the addition of 1 wt.% Ga. In Fig. 4a, the In-15wt.%Bi-35wt.%Sn alloy exhibits a microstructure with a relatively coarse distribution of phases, where the brighter phase corresponds to $BiIn_2(Sn)$ with the highest Bi concentration and the darker areas represent a mixture of β(In-rich) and γ(Sn-rich) phases. Since In and Sn have atomic numbers of 49 and 50, respectively, the contrast of the β(In-rich) and γ(Sn-rich) phases is low in BSE images. Generally, the β(In-rich) phases are darker and larger, while the γ(Sn-rich) phases are slightly brighter and smaller. The phases are labelled in Fig. 4 and can be clearly distinguished by the EDX mapping shown in Fig. 5.

With the addition of 1 wt.% Ga, as shown in Fig. 4b, the microstructure significantly changed, there is a decrease in the volume fraction of $BiIn_2(Sn)$ phase, the morphology

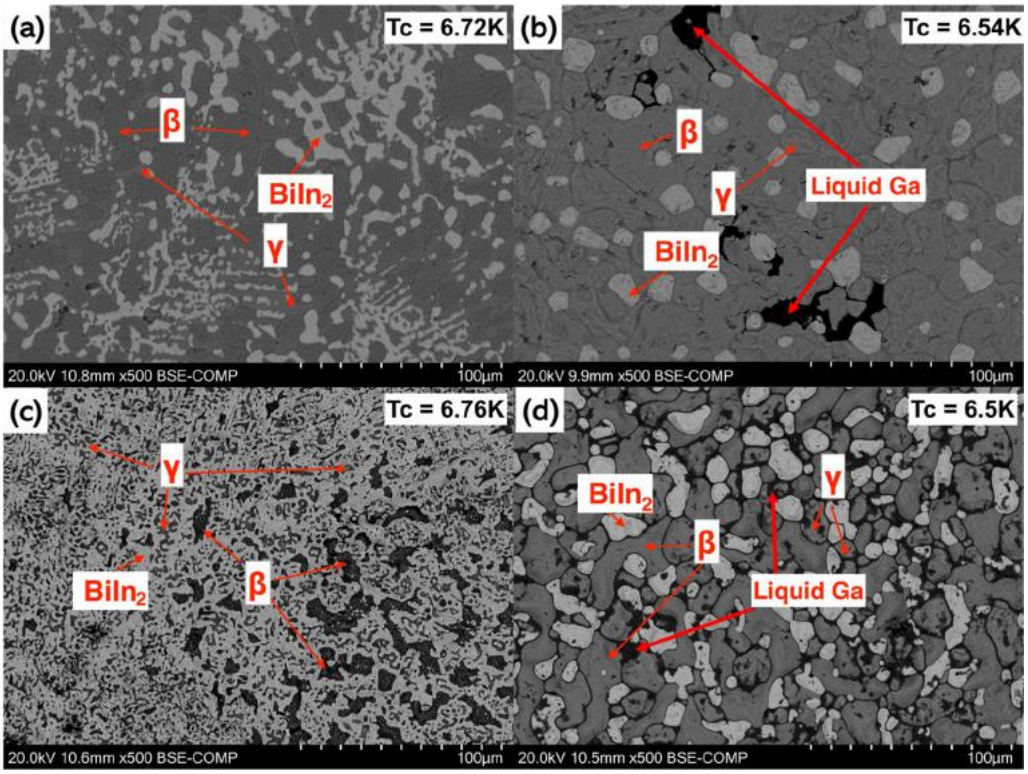

Fig. 4 SEM microstructural images of (a) In-15wt.%Bi-35wt.%Sn; (b) In-15wt.%Bi-35wt.%Sn with 1wt.%Ga addition; (c) In-23wt.%Bi-27wt.%Sn; (d) In-23wt.%Bi-27wt.%Sn with 1wt.%Ga addition.

of $BiIn_2$(Sn) changed into a rod-like shape, and the grains of the $BiIn_2$(Sn) phase become more uniformly dispersed within the β and γ matrix. Compared to the sample without Ga addition, there are large dark areas associated with Ga detected by the EDX mapping in Fig. 5b. Being the last phase to solidify, Ga tends to be present at interfaces, such as grain boundaries of phases that are solidified beforehand. In In-15wt.%Bi-35wt.%Sn, Ga is pushed out to pockets that are inhomogeneously distributed in the β and γ matrix.

Similarly, comparing Fig. 4c and d, the In-23wt.%Bi-27wt.%Sn alloy without Ga shows a coarser microstructure with larger and more irregularly distributed darker β phases at the bottom right corner of the image and a much finer dark $\gamma+\beta$ phases distributed on the left side of the image. With the addition of 1 wt.% Ga in Fig. 4d, the volume fraction of $BiIn_2$(Sn) phases become smaller and grains become more evenly distributed within the β and γ matrix. The Ga in the In-23wt.%Bi-27wt.%Sn alloy tends to disperse along the grain boundaries rather than forming inhomogeneously distributed pockets as observed in the In-15wt.%Bi-35wt.%Sn+1wt.%Ga sample (Fig. 4b).

Combining the XRD data (Fig. 3) and DSC analysis (Fig. 1), the Ga addition plays an important role in enhancing the homogeneity of the microstructure, changing the solidification process and further changing the volume fraction of each of the intermetallic phases.

Superconducting properties

Figure 6a shows the electrical resistance of In-23wt.%Bi-27wt.%Sn with 1%Ga as a function of temperature in the range of 3–300 K at zero magnetic field. The resistance decreases with decreasing temperature from 300 K to 6.5 K, supporting the metallic behaviour of this sample. The resistance drops to zero at 6.5 K. Furthermore, a hysteresis around 270 K is observed in the heating and cooling curves and is likely attributed to phase transformations or solute redistribution among or within the three phases. Our previous study found that Bi solute atoms in the β or γ phases tend to approach thermodynamic equilibrium with temperature variations and this process also results in phase transformations between the $BiIn_2$ and β or γ phases.[13] Figure 6b shows the temperature dependence of resistance for In-23wt.%Bi-27wt.%Sn with 1wt.%Ga under an applied magnetic field of up to 0.2 T. As the magnetic field strength increases, the T_c decreases because the magnetic field disturbs the Cooper pairs and makes it harder to maintain superconductivity. Also, in type II superconductors like In-Bi-Sn, the magnetic field penetrates inside the material in the form of vortices.

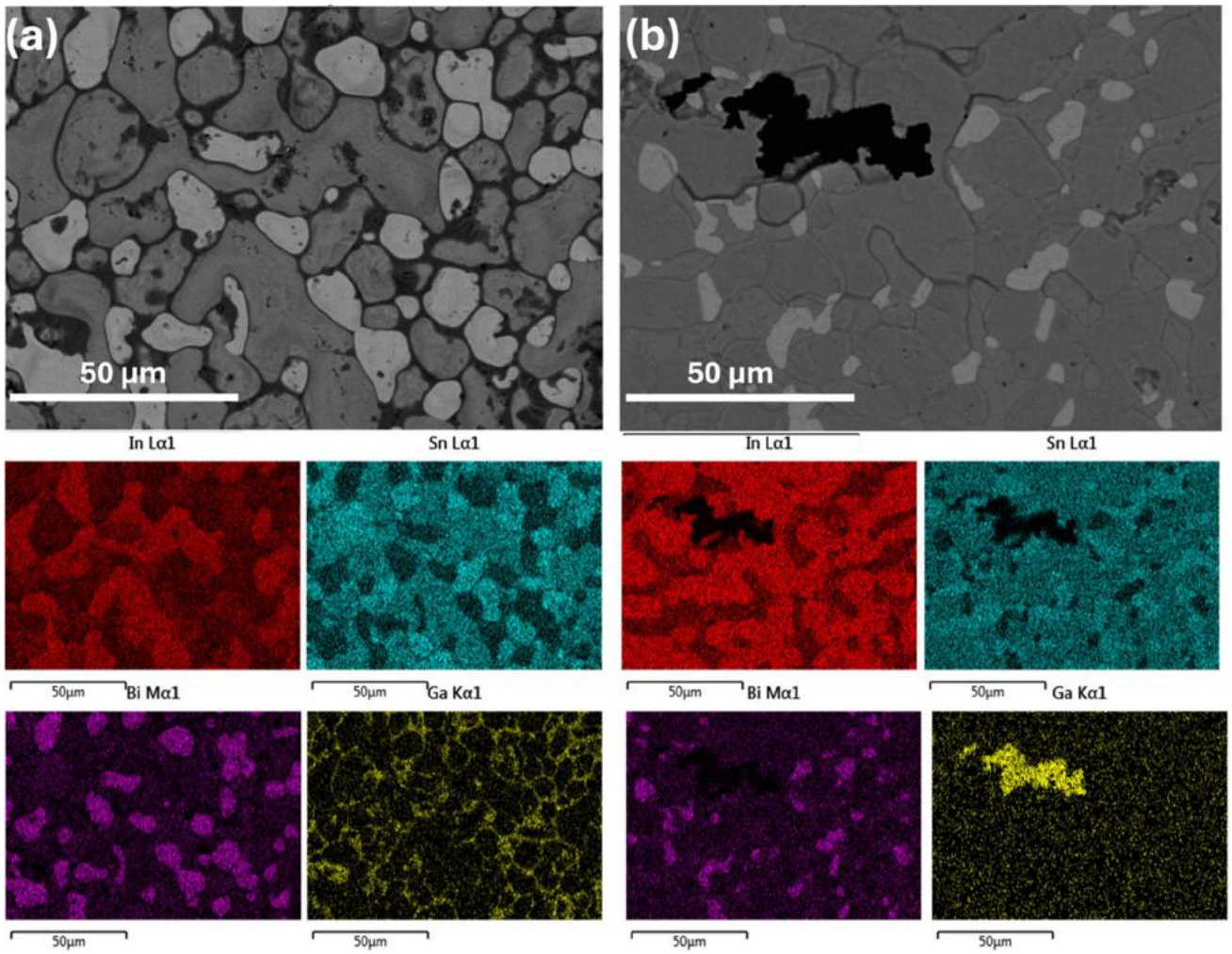

Fig. 5 SEM image and EDX mappings of (a) In-23wt.%Bi-27wt.%Sn with Ga addition, and (b) In-15wt.%Bi-35wt.%Sn with Ga addition.

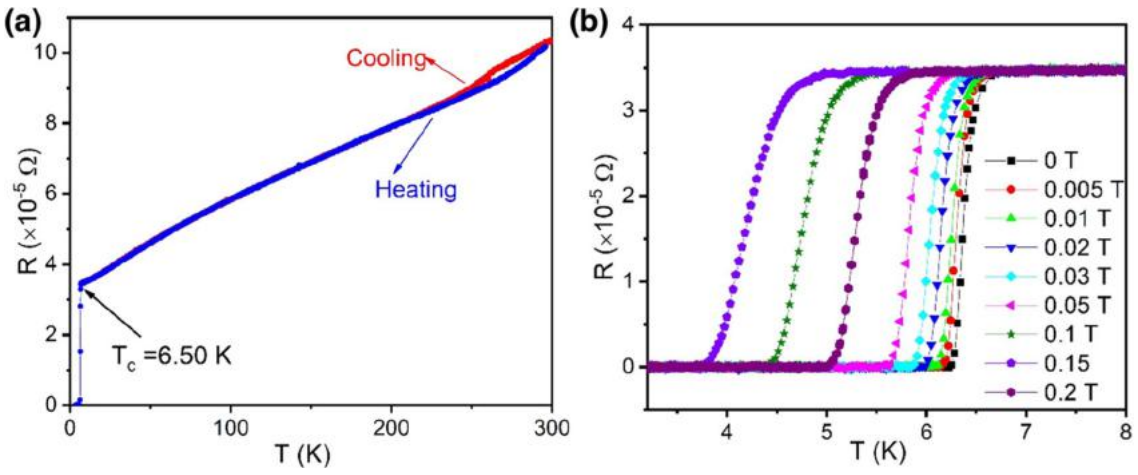

Fig. 6 (a) Temperature dependence of resistance for In-23wt.%Bi-27wt.%Sn with 1%wtGa. (b) Temperature dependence of resistance under different magnetic fields for the same sample (Color figure online).

The onset T_c shifts to lower temperatures with increasing magnetic field strength as the vortex density increases, indicating that the superconducting properties of this alloy are suppressed by the presence of applied magnetic fields, which is a common behaviour observed in most superconductors under typical working conditions.

The upper critical field, B_{c2}, is characterised as the field at which the electrical resistance becomes 90% of the normal state resistance. Figure 7 shows B_{c2} as a function of reduced temperature for both samples and 1% Ga-added counterparts. B_{c2} exhibits a linear temperature dependence for all samples. The estimated slopes for B_{c2} are 0.1304, 0.1055, 0.1237 and 0.1029 T/K for In-15wt.%Bi-35wt.%Sn, In-15wt.%Bi-35wt.%Sn with 1%Ga, In-23wt.%Bi-27wt.%Sn and In-23wt.%Bi-27wt.%Sn with 1% Ga, respectively. B_{c2} are estimated using one-band Werthamer–Helfand–Hohenberg (WHH) theory where $B_{c2}(0) = -0.69\ T_c\ (dB_{c2}/dT)$. The estimated B_{c2} values are 0.8763, 0.6899, 0.8362 and 0.6739 T for In-15wt.%Bi-35wt.%Sn, In-15wt.%Bi-35wt.%Sn with 1%Ga, In-23wt.%Bi-27wt.%Sn and In-23wt.%Bi-27wt.%Sn with 1% Ga, respectively. For both samples, B_{c2} decreases upon adding Ga. This is related to the reduction of the electron mean free path due to the enhanced scattering after Ga is added.

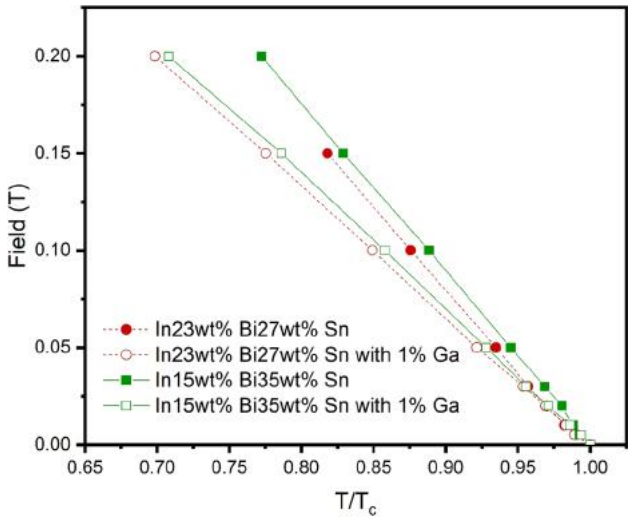

Fig. 7 Comparison of upper critical field H_{C2} among tested samples. Green: In-15wt.%Bi-35wt.%Sn based samples with 1wt.% Ga addition. Red: In-23wt.%Bi-27wt.%Sn based samples with 1wt.% Ga addition (Color figure online).

Figure 8a shows magnetic hysteresis loops of both samples and 1% Ga-added counterparts at 5 K. The magnetic moment of both samples is decreased after adding 1% Ga over the entire range of the magnetic field. Figure 8b shows the calculated J_c for In-23wt.%Bi-27wt.%Sn, In-15wt.%Bi-35wt.%Sn and 1% Ga-added counterpart samples at 5 K. For both compositions, the Ga added sample exhibits reduced J_c performance. As can be seen from Fig. 8b, J_c is as high as 0.51×10^4 A/cm^2 at 0.006 T for In15Bi35Sn and then reduced to 0.43×10^4 A/cm^2 at 0.006 T and 5 K. Similar behaviour was observed for the In-23wt.%Bi-27wt.%Sn sample. In-23wt.%Bi-27wt.%Sn (solid red circle), which has a different volume fraction of each phase and 26.97 % of the β-phase at room temperature (as shown in Table III), shows lower J_c of 0.45×10^4 A/cm^2 compared with 0.5×10^4 A/cm^2 for In-15wt.%Bi-35wt.%Sn with 37.96% β-phase This is in good agreement with a previous study by Mousavi et al.[7] Furthermore, the J_c decreases more rapidly with an increase in the applied magnetic field for samples with Ga addition. This indicates that Ga addition affects the flux pinning properties, leading to a reduced critical current density under both lower and higher magnetic fields. Similarly, samples with Ga addition (Fig. 6c and g) show narrower hysteresis loops at 5 K compared to the base samples, indicating weaker superconducting properties. Since the β phase and $BiIn_2$ phase has better superconducting properties than the

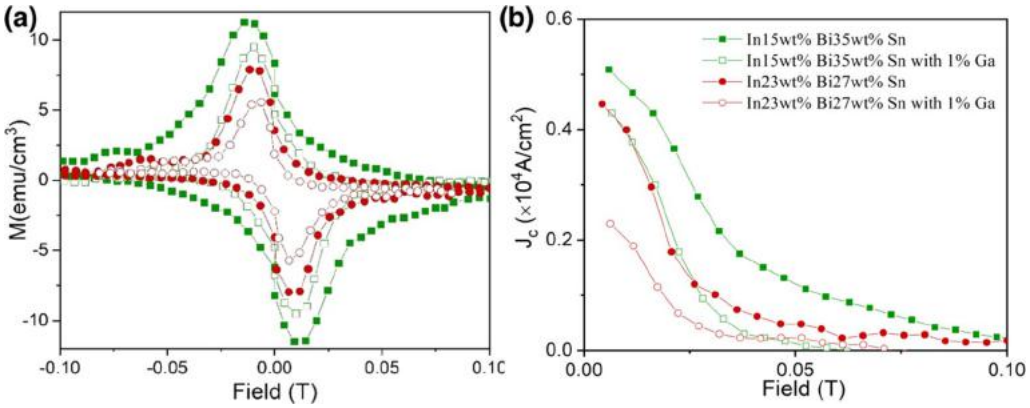

Fig. 8 (a) Temperature dependence of magnetic hysteresis loops at 5 K for In-23wt.%Bi-27wt.%Sn, In-15wt.%Bi-35wt.%Sn and 1% Ga-added counterparts and (b) corresponding J_C as a function of the applied magnetic field as indicated in the figure legend (Color figure online).

γ phase,[7,10] and Ga addition increases the volume fraction of the γ phase, which results in decay in the critical temperature and a lower J_c (Table III).

The tested In-15wt.%Bi-35wt.%Sn has a T_c at 6.72 K, which is similar to the value reported in the previous study,[7] and the In-23wt.%Bi-27wt.%Sn sample has a slightly higher T_c at 6.76 K, while the critical temperature of both samples decreases with Ga addition. Overall, the observed reduction in the B_{c2}, J_c and T_c in Ga-containing In-Sn-Bi solder alloys indicates that Ga negatively impacts their superconducting properties by altering the microstructural features of these alloys, such as introducing a phase with worse superconducting properties. These changes are particularly unfavourable, potentially disrupting the electron movement and flux pinning properties which are essential for superconductivity.

Pinning Mechanisms

To evaluate the impact of grains and interphase boundaries on the superconducting properties, EBSD mapping was carried out for the In-23wt.%Bi-27wt.%Sn sample, which has the highest critical temperature. Figure 9 shows the phase mapping and EBSD inversed pole figure (IPF) mapping of the grain orientation in this sample. The phases identified in Fig. 9a are consistent with those in the XRD patterns shown in Fig. 3, with a similar phase pattern containing β, γ and $BiIn_2$. Furthermore, the volume fraction of each phase from the phase map is similar to the Thermo-Calc prediction displayed in Table III. The phase map shown in Fig. 9a comprises three phases: 27.7% of β, 40.3% of γ and 32% of $BiIn_2$ (in volume fraction), compared to 26.97% of β, 31.00% of γ and 42.03% of $BiIn_2$ predicted by Thermo-Calc (shown in Table III), indicating the sample underwent a potential phase transformation during the experiment or sample preparation. As shown in Fig. 9b, the grains of In-23wt.%Bi-27wt.%Sn exhibit a random orientation, with a more pronounced recrystallisation observed within the γ phase than the other two phases.

Compared to the SEM microstructure, the EBSD map shows a finer scale of grain size especially within the γ phase compared to the phase map, suggesting that a higher density of grain boundaries exists in the sample that will contribute to the flux pinning. In this sample, the recrystallisation of the γ phase is more pronounced; however, since the microstructure can vary across different samples, it remains unclear which phase is more prone to recrystallisation under specific conditions. Furthermore, these small grains are related to the recrystallisation which may be caused by the sample

Table III Summary of the superconducting properties and volume fraction of each phase at 20°C in tested samples (latter are calculated by Thermo-Calc 2024a using database TCSLD4: Solder Alloy v4.1)[15]

Sample	T_c (K) from ZFC and FC	T_c (K) from resistivity	J_c (A/cm^2) at 5 K & 0.06 T	dB_{c2}/dT (T/K)	B_{c2} (T)	% β-phase	% γ-phase	% $BiIn_2$
In-15wt.%Bi-35wt.%Sn	6.31	6.72	0.51×10^4	0.1304	0.88	37.96	38.79	23.25
In-15wt.%Bi-35wt.%Sn with 1%Ga	5.93	6.54	0.43×10^4	0.1055	0.69	–	–	–
In-23wt.%Bi-27wt.%Sn	6.27	6.76	0.44×10^4	0.1237	0.84	26.97	31.00	42.03
In-23wt.%Bi-27wt.%Sn with 1%Ga	6.31	6.55	0.23×10^4	0.1029	0.67	–	–	–

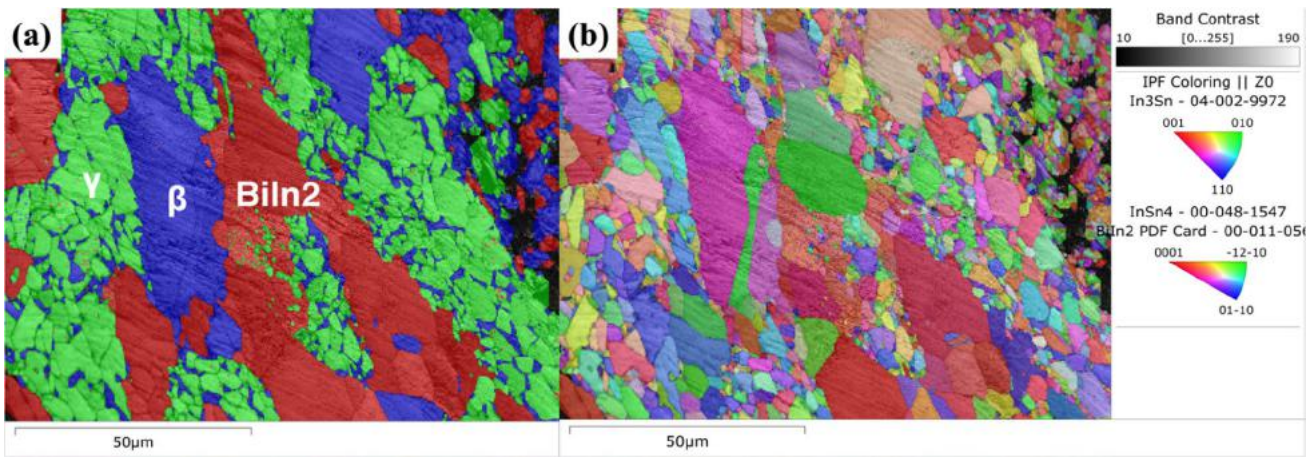

Fig. 9 EBSD maps of In-23wt.%Bi-27wt.%Sn sample: (a) phase map; (b) inverse pole figure (IPF) map (Color figure online).

preparation and may not happen in the solidified sample without any heat treatment. The microstructural characteristics here provide us with new insight suggesting that it is possible to enhance superconducting properties using heat treatment in In-Bi-Sn low-temperature solder alloys. In these alloys, grains may undergo significant recrystallisation after heat treatment due to a higher homologous temperature at ambient conditions, leading to an increase in grain boundaries that contribute to flux pinning. Also, the phase transformation at higher temperature can cause more Bi solute atoms to dissolve in the β, resulting in better superconducting properties. Notably, shorter heat treatment durations or lower temperatures may be required to achieve the desired recrystallisation effects without promoting significant grain growth. Dynamic recrystallisation with applied strain may also help to achieve the desired microstructure.

Conclusion

Combining the discussion and all experimental data in this paper, several conclusions can be drawn:

- Adding Ga to In-Bi-Sn solder alloys generally results in a degradation of their superconducting properties in all aspects including lower critical temperatures (T_c), critical current densities (J_c) and upper critical fields (H_c). The Ga addition significantly modifies the microstructure of the alloys, particularly by increasing the volume fraction of the γ phase and introducing a Ga phase which has poor superconducting properties.
- The role of grain boundaries as effective pinning centres is very important; however, the addition of Ga alters the distribution and characteristics of these boundaries within the microstructure, weakening their effectiveness in pinning magnetic flux lines. Furthermore, the grain boundaries and microstructure can be further refined by heat treatment for these alloys, potentially leading to a higher pinning force density.
- For future work, to enhance superconducting properties in the In-Bi-Sn system, the use of a trace element that either suppresses the formation of the γ phase, acts as solute atoms dissolved in the β or $BiIn_2$ lattices, or refines the microstructure during solidification or at lower temperatures through heat treatment should be considered. Additionally, adjusting cooling rates or applying specific heat treatments may also help achieve desired microstructural features.

Acknowledgments We wish to acknowledge (1) the Centre for Microscopy and Microanalysis at the University of Queensland for facilities, instruments (Hitachi SU3500SEM, JEOL cross-section polisher, JEOL 7800 SEM, Bruker D8 Advance x-ray diffractometer), and scientific and technical assistance from Ms Anya Yago; (2) Nihon Superior Company Ltd. for their support of this research and the supply of the indium ingots; (3) the Central Analytical Research Facility (CARF) at Queensland University of Technology for instruments and facilities.

Funding This research was funded by the Australian Research Council (ARC), Australia [LP210301248]; the University of Queensland Research Training Program Stipend.

Conflict of interest ARC Linkage project [LP210301248] received funding from Nihon Superior Co., Ltd. (Japan).

References

1. Y. Tsui, R.A. Mahmoud, E. Surrey, and D. Hampshire, *IEEE Trans. Appl. Supercond.* 26, 1 (2016). https://doi.org/10.1109/TASC.2016.2536806.
2. O.A. Ogunseitan, *JOM* 1989(59), 12 (2007). https://doi.org/10.1007/s11837-007-0082-8.
3. M.S. Chang, M.A.A. Mohd Salleh, and D.S.C. Halin, *IOP Conf. Ser.: Mater. Sci. Eng.* 957, 12059 (2020). https://doi.org/10.1088/1757-899X/957/1/012059.
4. T. Murakami, H. Arima, and Y. Mizuguchi, *AIP Adv.* 13, 125008 (2023). https://doi.org/10.1063/5.0183526.
5. J.E. Evetts and J.M.A. Wade, *J. Phys. Chem. Solids* 31, 973 (1970). https://doi.org/10.1016/0022-3697(70)90308-2.
6. C. Aksoy, T. Mousavi, G. Brittles, C.R.M. Grovenor, and S.C. Speller, *IEEE Trans. Appl. Supercond.* 26, 1 (2016). https://doi.org/10.1109/TASC.2016.2539423.
7. T. Mousavi, C. Aksoy, C.R.M. Grovenor, and S.C. Speller, *Supercond. Sci. Technol.* 29, 15012 (2015). https://doi.org/10.1088/0953-2048/29/1/015012.
8. S.F. Bartram, W.G. Moffatt, and B.W. Roberts, *J. Less-Common Metals* 62, 9 (1978). https://doi.org/10.1016/0022-5088(78)90011-5.
9. T. Mousavi, W. Darby, C. Aksoy, T. Davies, G. Brittles, C. Grovenor, and S. Speller, *MRS Adv.* 1, 3483 (2016). https://doi.org/10.1557/adv.2016.435.
10. J.H. Wernick and B.T. Matthias, *J. Chem. Phys.* 34, 2194 (1961). https://doi.org/10.1063/1.1731856.
11. C. Aksoy, B. Çakır, E.T. Koparan, C. Şimşek, E. Tıraşoğlu, S. Speller, C.R.M. Grovenor, T. Küçükömeroğlu, and E. Yanmaz, *Supercond. Sci. Technol.* 36, 15007 (2023). https://doi.org/10.1088/1361-6668/aca62b.
12. T.-T. Zhang, G.-X. Xie, G.-T. Cheng, S.-H. Chen, D.-Y. Zhu, Y.-R. Zhang, W.-P. Han, D. Chen, and Y.-Z. Long, *J. Mater. Sci. Mater. Electron.* 33, 10021 (2022). https://doi.org/10.1007/s10854-022-07993-5.
13. J. Zhou, X.F. Tan, S.D. McDonald, and K. Nogita, *Materials*, 17, 3669 (2024). https://doi.org/10.3390/ma17153669
14. J.C. Slater, *J. Chem. Phys.* 41, 3199 (1964). https://doi.org/10.1063/1.1725697.
15. J.O. Andersson, T. Helander, L. Höglund, P. Shi, and B. Sundman, *Calphad* 26, 273 (2002). https://doi.org/10.1016/S0364-5916(02)00037-8.